Optics Letters

Electrically induced adiabatic frequency conversion in an integrated lithium niobate ring resonator

Xiaotong He,* Luis Cortes-Herrera, Kwadwo Opong-Mensah, Yi Zhang, Meiting Song, Govind P. Agrawal, and Jaime Cardenas

The Institute of Optics, University of Rochester, Rochester, New York 14627, USA
**Corresponding author: xhe20@ur.rochester.edu*

Received 17 August 2022; revised 5 October 2022; accepted 15 October 2022; posted 17 October 2022; published 7 November 2022

Changing the frequency of light outside the laser cavity is essential for an integrated photonics platform, especially when the optical frequency of the on-chip light source is fixed or challenging to be tuned precisely. Previous on-chip frequency conversion demonstrations of multiple GHz have limitations of tuning the shifted frequency continuously. To achieve continuous on-chip optical frequency conversion, we electrically tune a lithium niobate ring resonator to induce adiabatic frequency conversion. In this work, frequency shifts of up to 14.3 GHz are achieved by adjusting the voltage of an RF control. With this technique, we can dynamically control light in a cavity within its photon lifetime by tuning the refractive index of the ring resonator electrically.

https://doi.org/10.1364/OL.473113

Changing the frequency of light outside the laser cavity is critical in an integrated photonics platform especially when the optical frequency of the on-chip light source is fixed or cannot be tuned precisely. For example, individual single-photon sources from quantum dots [1] and color centers [2] have inhomogeneous broadening of multiple GHz, which makes it challenging to build quantum circuits using many of them. The emergence of frequency-modulated continuous wave lidar (FMCW lidar) [3,4] demands continuous frequency modulation of the light frequency during operation. All these applications require a robust on chip method to tune the frequency of light continuously after the device is fabricated.

Frequency conversion of multiple GHz can be done by leveraging the electro-optic effect, acousto-optic effect, and spectral shearing [5,6]. However, the on-chip demonstrations of these methods have limitations when tuning the shifted frequency continuously. The frequency conversion based on typical electro-optic phase modulation (PM) generates additional sidebands [7] and, intrinsically, cannot reach a high conversion efficiency. Even in single-sideband demonstrations [8], the theoretical maximum frequency conversion efficiency is less than 34%. A frequency shifter based on electro-optical modulation in the lithium niobate on insulator (LNOI) platform has shown near unity efficiency and frequency shifts of up to hundreds of GHz [9]. In this device, the frequency shifts are constrained to integer multiples of the doublet splitting of the coupled resonator, which is fixed during device fabrication, and limits the device's tunability. The frequency can also be shifted via the acousto-optic effect. However, the frequency shift shown in previous demonstrations [10] in lithium niobate (LN) cannot be tuned because it depends on the interdigital transducer (IDT) and Bragg angle, which are fixed during device fabrication. Spectral shearing in an optomechanical single-photon frequency shifter [6] shows tunable single-photon frequency shifts of up to 150 GHz, which are achieved by changing the drive phase, but it requires synchronization of the photon arrival time and the RF signal. The confinement of the mechanical wave is achieved with suspended waveguides.

Adiabatic frequency conversion (AFC) [11–17] is a promising alternative method for continuous frequency shifting. In AFC, light excites an optical cavity mode, then the cavity's refractive index is modulated to shift its resonant frequency within the photon lifetime. Light trapped inside the cavity follows the cavity's instantaneous resonance frequency [12]. In previous works, on-chip AFC was demonstrated in silicon ring resonators and photonic crystal cavities by carrier injection via a *p-i-n* junction [11] or absorption of an optical pump from outside the chip [14,16]. However, carrier injection introduces optical losses [11,14,16] which reduce the cavity's photon lifetime and hence limits the conversion efficiency. It also requires a femtosecond time scale high-power pulsed laser or lossy schemes for carrier extraction or injection, which limit the scalability of an AFC platform. AFC was recently demonstrated in a whispering gallery resonator in bulk MgO-doped lithium niobate crystal [15], using the Pockels effect, which is fundamentally lossless. Due to the size of the whispering gallery resonator, the electrodes cannot be placed near each other. Thus, the electrical-optical efficiency is limited and only up to 5 GHz of frequency shift can be achieved when applying 20 V of voltage.

In this Letter, we demonstrate electrically induced adiabatic frequency conversion in an LNOI integrated photonic platform. Lithium niobate exhibits a large electro-optic effect, which allows instantaneous, lossless modulation of its refractive index. The LNOI platform enables high-quality factor resonators [18,19] with photon lifetimes of 4 ns (Q~10^7) [19]. The high index contrast of the LNOI platform not only greatly reduces the device's footprint, but also increases the electro-optical efficiency. In our device, the frequency of the shifted light is not set upon fabrication but can be tuned by the amplitude of the RF

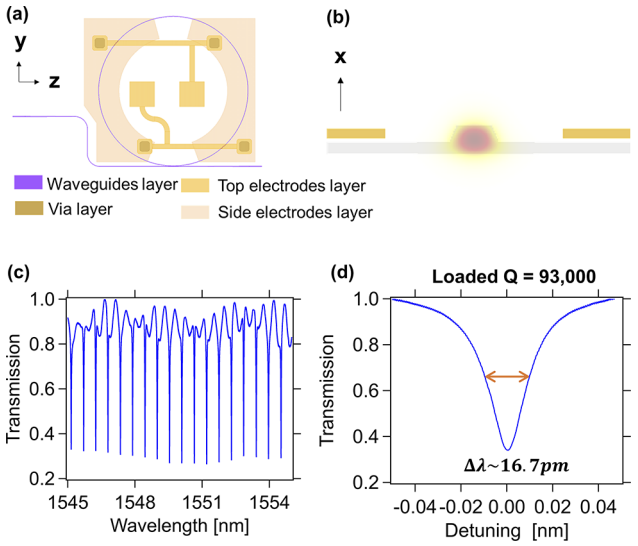

Fig. 1. (a) Schematic of the AFC device. The waveguide layer consists of a bus waveguide and a ring resonator. Side electrodes generate an electric field along lithium niobate's crystallographic z axis. (b) Cross section of the fundamental TE mode of the bus waveguide. (c) Measured spectrum. (d) Zoom-in of the resonance at 1551.75 nm. The FWHM is calculated at the midpoint between the maximum and minimum of the resonance.

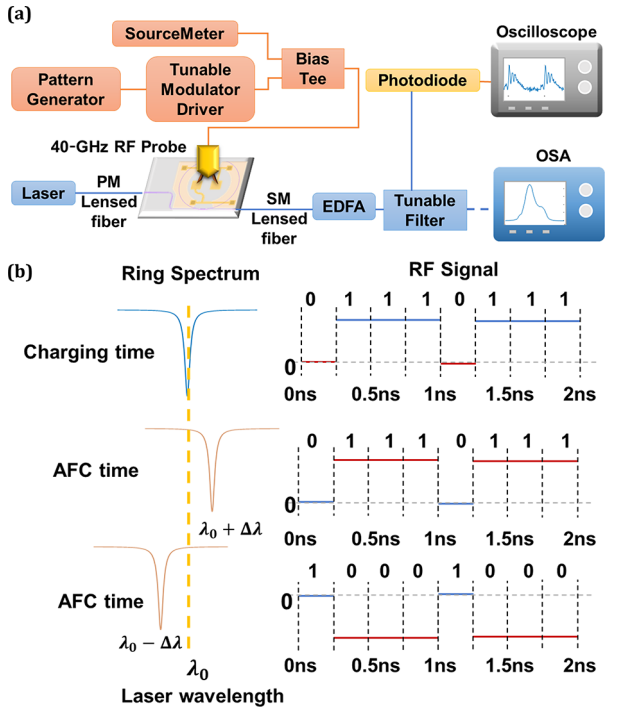

Fig. 2. (a) Experimental setup. We use an oscilloscope to check the beating signal and use an OSA to check the spectrum of the output. (b) When setting the RF pattern to be "1110," the ring is charged up during the "0" period. During the "1" period, a voltage is applied, and the ring's resonance is shifted. The light trapped inside undergoes AFC. We set the pattern to "1000" to invert the direction of the applied electric field and change the direction of the frequency shift.

control. This allows a continuous and dynamic control of the laser frequency.

We fabricate a ring resonator with a 300-μm radius [Fig. 1(a)] on the LNOI platform. The waveguide layer consists of a bus waveguide and a ring resonator that are patterned through e-beam lithography and etched with ion milling. We choose an LNOI substrate that consists of a 600-nm layer of X-cut lithium niobate (LN) on 4.7 μm of thermal SiO_2 on a 0.5-mm-thick silicon substrate. The bus is a single-mode ridge waveguide with a top width of 1 μm, an etch depth of 350 nm, and a slab thickness of 250 nm [Fig. 1(b)]. The waveguide design ensures that polarization coupling between the TE_0 and TM_0 modes is inhibited by a large difference between their propagation constants. This, in turn, allows the resonance to be excited by pure TE or pure TM polarization [20]. The waveguide width is tapered from 3.5 μm to 1 μm at the edges of the chip to obtain a higher edge-coupling efficiency from the fiber to the device [21,22]. We use hot piranha and RCA-1 silicon wafer cleaning processes to remove the micro masking and resist residues. After defining the waveguides, we deposit 100 nm of SiO_2 through plasma-enhanced chemical vapor deposition (PECVD) to protect the waveguide. To induce electro-optical modulation, metallic side electrodes surround the waveguide forming the ring resonator. We balance the quality factor and the electro-optic efficiency by setting the electrode separation to 4.6 μm. These side electrodes generate an electric field along the z direction of the LN crystal to use its largest electro-optic coefficient (r_{33} = 30.8 pm/V). To ensure precision in the distance between the waveguide and the metallic electrodes, the side electrodes are defined with e-beam lithography and lift-off of 300 nm of evaporated Pt with Cr as an adhesion layer. Double-spun PMMA and evaporation reduce debris during the lift-off. Two-micron-thick PECVD SiO_2 is then deposited as the cladding layer. Vias are patterned with photolithography, and reactive ion etching (RIE) is used to etch the SiO_2 until the electrode layer is fully exposed. The top electrodes, which connect the two side electrodes and serve as contact pads to the probes, are patterned with photolithography and deposited with 400 nm of sputtered platinum followed by lift-off. Instead of dicing through the waveguide or polishing, we etch the facet of the device to obtain a higher edge coupling. The fabricated device shows an intrinsic quality factor of 117 k (the fitted data can be found in Supplement 1) and a loaded quality factor of 93 k, i.e., a photon lifetime of 0.1 ns [Figs. 1(c) and 1(d)]. The calculated intrinsic quality factor corresponds to a propagation loss of approximately 3.34 dB/cm. The state-of-the-art value is 2.7 dB/m for a waveguide width of 2.4 μm that does not have surrounding electrodes [19].

We measure a frequency shift of 11 GHz of the laser light by driving the ring resonator with an RF control of 6.5 V at 4 GHz. To measure AFC, we perform the following process. First, we set the tunable laser into one of the ring resonances at 1551.7490 nm. Then, we use a gain-tunable modulator driver to amplify an RF control generated with a 40-GHz pattern generator [Fig. 2(a)]. With a bias tee, we combine a DC voltage from a Source-Meter (Keithley) to compensate the DC offset from the modulator driver. The RF control is applied to the device through a 40-GHz RF probe. We set the frequency of the pattern generator to be 4 GHz with the pattern of "1110" [Fig. 2(b)], which is repeated every 1 ns. During the "0" period, the ring resonator is charged with the input light, and during the "1" period, the control voltage is applied to the ring resonator. When the voltage is applied, the refractive index of the ring resonator changes, the light trapped in the cavity undergoes AFC, and the frequency of

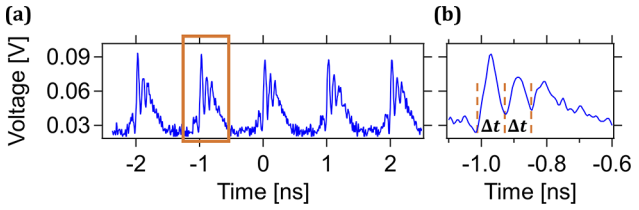

Fig. 3. (a) Observed signal pattern. (b) Enlarged view of the beating signal. We calculate the converted wavelength by measuring the beating period Δt.

the light is shifted. The frequency-shifted light interferes with the original light from the laser at the transmission port and generates an optical beat signal at the detector. To characterize the beat signal, we amplify the light from the through port with an erbium-doped fiber amplifier (EDFA) and remove the amplified spontaneous emission noise with a tunable filter. We use the EDFA to make the optical beating signal strong enough to be detected by our receiver/electronics setup. The EDFA is not necessary for AFC to take place, nor does it affect its efficiency. The amplified signal is detected by a 40-GHz *p-i-n* photodiode and then sent to a real-time oscilloscope to display the pattern. The pattern we observe shows the beating signal indicating that more than one frequency of light is impinging on the detector (Fig. 3).

The beating signal pattern can be described by [15]

$$S_D = I_L + I_{AFC}\exp(-\frac{t}{\tau}) + 2\sqrt{I_L I_{AFC}}\cos(2\pi\Delta\nu t + \phi_0)\exp(-\frac{t}{2\tau}). \quad (1)$$

Here, I_L is the intensity of the unshifted laser in the bus waveguide; I_{AFC}, the intensity of frequency-shifted light; τ, the photon lifetime; $\Delta\nu$, the induced frequency shift $\Delta\nu = |\nu_L - \nu_{AFC}|$; and ϕ_0, the initial phase term when the beat starts. The beating signal decays in ~0.25 ns during each period, which agrees with the estimated photon lifetime of ~0.1 ns. We observe a beating period Δt of 90 ps (Fig. 3), which corresponds to a beat note $\Delta\nu = \frac{1}{\Delta t}$ and a frequency shift of 11 GHz with a 6.5 V control, or a wavelength conversion of approximately 88 pm in vacuum. The limit for adiabatic frequency conversion is that the lifetime is longer than the rise time of the RF signal. The rise time for our RF signal is 14 ps. The photon lifetime of 0.1 ns is much longer than the rise time of the RF signal.

We demonstrate frequency conversion to both shorter and longer wavelengths by changing the sign of the refractive index change. We connect the optical signal from the tunable EDFA filter directly to an optical spectrum analyzer (OSA) to observe the converted wavelength spectrum. When we set the pattern to be "1110", the change in refractive index is positive and the wavelength is converted to longer wavelengths, i.e., lower frequency. We then invert the sign of the refractive index change by setting the pattern to be "1000" and adjusting the DC bias. The optical spectrum shows that the wavelength is converted to shorter wavelengths, i.e., higher frequency [Figs. 4(a) and 4(b)]. The frequency shift in adiabatic frequency conversion has a single sideband compared to regular electro-optic modulation which produces two. For this reason, we observe only one shifted frequency shoulder in Figs. 4(a) and 4(b). Because the period of "1" (the period for AFC process is 0.75 ns) is much longer than the photon lifetime (0.1 ns), for most of the time, the OSA is receiving the original wavelength directly from the laser.

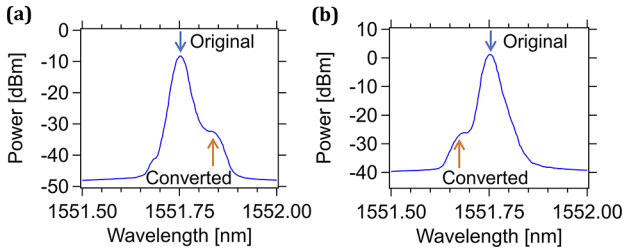

Fig. 4. Light is converted (a) into a longer wavelength when we set the RF pattern to be "1110" and (b) into a shorter wavelength when setting the RF pattern to be "1000."

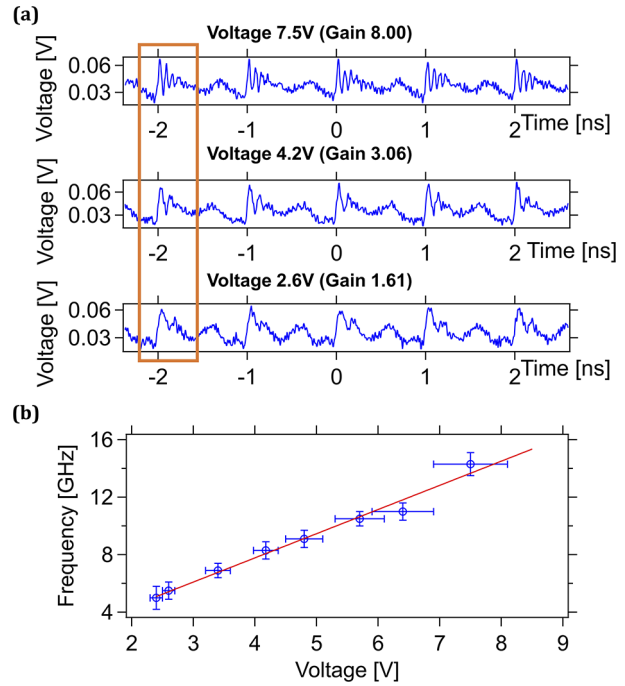

Fig. 5. (a) Beat signals stretch when we decrease the voltage. (b) Frequency shift change with applied voltage.

That is why the peak of the original wavelength is much higher than the peak of the converted light. The wavelength conversion measured in Figs. 4(a) and 4(b) is 0.09 ± 0.02 nm (limited by the accuracy of the OSA), which corresponds to a frequency conversion of $\Delta\nu = \frac{c}{\lambda^2}\Delta\lambda = 11.2 \pm 2.5$ GHz. The measurement is done at a drive voltage of 6.5 V, which corresponds to a gain of 7.46. This result is in good agreement with the conversion measured using the beating period (11.0 ± 0.6 GHz) of the signal shown in Fig. 5(b).

We further confirm the frequency shift is due to AFC by varying the applied RF voltage and demonstrate tunable frequency conversion using the same 4-GHz "1110" RF pattern. Unlike conventional electro-optic modulation, where the magnitude of the frequency shift is determined by the RF modulation frequency, the frequency shift due to AFC is determined by the amplitude of the applied voltage. Thus, to verify that the phenomenon we observe is the result of AFC, we modify the gain of the modulator driver to change the amplitude of the RF control, while maintaining the 4-GHz "1110" pattern. We characterize the output voltage amplitude of the modulator driver as a function of gain by measuring the peak-to-peak voltage from the

modulator driver on the oscilloscope and recording the corresponding gain shown on the modulator driver. By tuning the amplitude of the RF voltage, we successfully tune the frequency of the converted light [Fig. 5(a)]. As we decrease the gain of the voltage, the beat note frequency also decreases, indicating a lower frequency shift of light. We measure frequency shifts of 14.3, 8.3, and 5.5 GHz for voltage amplitudes of 7.5 V, 4.2 V, and 2.6 V, respectively [Fig. 5(a)]. The linear relationship of the voltages and the corresponding vacuum wavelength conversion is shown in Fig. 5(b).

The conversion efficiency of AFC can be calculated as [23]

$$\eta = \frac{27}{4}\frac{\gamma_e^2\gamma_0}{\gamma^3}[1-\exp(-\gamma t_0)]^2 = \frac{27}{4}\frac{Q^3}{Q_e^2 Q_0}[1-\exp(-\gamma t_0)]^2. \tag{2}$$

The modeling and derivation of this equation can be found in detail in Ref. [23]. Here, γ_0 is the intrinsic decay rate and γ_e is the extrinsic decay rate, the mode's decay rate γ is given by $\gamma = \gamma_e + \gamma_0$. In our device, the loaded quality factor Q is 93 k; the intrinsic quality factor Q_0 is 117 k, and the modulation time t_0 is 0.75 ns. The calculated conversion efficiency of our device is 22.6%. The maximum efficiency occurs when $Q_0 = 2Q_e$, which makes the ratio $\frac{27}{4}\frac{Q^3}{Q_e^2 Q_0}$ equal to 1.

In conclusion, for the first time to the best of our knowledge, we demonstrate electrically induced frequency shifts of light through adiabatic frequency conversion in an integrated LN platform that is fundamentally lossless. The operation bandwidth of the device is 2 GHz due to the 2 GHz ring resonator linewidth. Since the AFC phenomenon is ensured as long as the photon lifetime is longer than the RF signal rise time, we believe that the performance of our device can be further optimized. The extent of frequency conversion is constrained by the electro-optic efficiency, which is limited by the minimum separation of the metal electrodes. The electro-optic efficiency increases as the electrode separation decreases. However, the absorption loss to the electrodes increases as their separation decreases, too. Assuming a quality factor of approximately 90,000 as the lower limit for achieving AFC, we calculate the gap at which the loss is dominated by the electrode separation to be 3.2 μm. These conditions can be achieved by improving the fabrication process and redesigning the device. Lithium niobate has a broad transparency window [24] so our method can also be applied to visible and NIR wavelengths. The optical mode is more confined at shorter wavelengths and the electrodes can be placed closer to the waveguide and achieve higher frequency conversion. The calculated frequency conversion for shorter wavelengths is shown in Supplement 1 (Fig. S3). In [23], the authors find that the maximum efficiency occurs when $Q_0 = 2Q_e$, or in terms of the decay rate, $\gamma_e = 2\gamma_0$. Optimizing the gap between the bus waveguide and the resonator to achieve the $\gamma_e = 2\gamma_0$ condition will maximize the conversion efficiency.

Our work enables tuning the shifted frequency of light by adjusting the applied voltage on a lossless, on-chip scalable photonic platform. The on-chip resonator enables an order of magnitude higher electro-optic efficiency (than bulk counterparts [15]) on a scalable platform. Adiabatic frequency conversion does not generate unwanted sidebands like traditional electro-optic modulators and frequency combs; and does not need a high-power optical pump like previous AFC demonstrations. The tunability feature paves the way for potential applications in quantum dots and color centers. Considering that the inhomogeneous broadening of individual color centers and quantum dot emission is approximately tens of GHz [1,2], the demonstrated frequency conversion has the potential to align the emission of different color centers to specific frequencies. The tunability of over ±14.3 GHz by changing the drive voltage has the potential for compact on-chip integration of FMCW lidar.

Funding. National Science Foundation (ECCS-1807735).

Disclosures. The authors declare no conflicts of interest.

Data availability. Data underlying the results presented in this paper are not publicly available at this time but may be obtained from the authors upon reasonable request.

Supplemental document. See Supplement 1 for supporting content.

REFERENCES

1. J. S. Wildmann, R. Trotta, J. Martín-Sánchez, E. Zallo, M. O'Steen, O. G. Schmidt, and A. Rastelli, Phys. Rev. B **92**, 235306 (2015).
2. J. L. Zhang, K. G. Lagoudakis, Y.-K. Tzeng, C. Dory, M. Radulaski, Y. Kelaita, K. A. Fischer, S. Sun, Z.-X. Shen, and N. A. Melosh, Optica **4**, 1317 (2017).
3. A. Martin, D. Dodane, L. Leviandier, D. Dolfi, A. Naughton, P. O'Brien, T. Spuessens, R. Baets, G. Lepage, P. Verheyen, P. De Heyn, P. Absil, P. Feneyrou, and J. Bourderionnet, J. Lightwave Technol. **36**, 4640 (2018).
4. F. Zhang, L. Yi, and X. Qu, Opt. Commun. **474**, 126066 (2020).
5. L. J. Wright, M. Karpiński, C. Söller, and B. J. Smith, Phys. Rev. Lett. **118**, 023601 (2017).
6. L. Fan, C.-L. Zou, M. Poot, R. Cheng, X. Guo, X. Han, and H. X. Tang, Nat. Photonics **10**, 766 (2016).
7. M. Izutsu, S. Shikama, and T. Sueta, IEEE J. Quantum Electron. **17**, 2225 (1981).
8. H.-P. Lo and H. Takesue, Optica **4**, 919 (2017).
9. Y. Hu, M. Yu, D. Zhu, N. Sinclair, A. Shams-Ansari, L. Shao, J. Holzgrafe, E. Puma, M. Zhang, and M. Lončar, Nature **599**, 587 (2021).
10. L. Shao, N. Sinclair, J. Leatham, Y. Hu, M. Yu, T. Turpin, D. Crowe, and M. Lončar, Opt. Express **28**, 23728 (2020).
11. T. Tanabe, E. Kuramochi, H. Taniyama, and M. Notomi, Opt. Lett. **35**, 3895 (2010).
12. M. Notomi and S. Mitsugi, Phys. Rev. A **73**, 051803 (2006).
13. B. A. Daniel, D. N. Maywar, and G. P. Agrawal, Opt. Lett. **36**, 4155 (2011).
14. S. F. Preble, Q. Xu, and M. Lipson, Nat. Photonics **1**, 293 (2007).
15. Y. Minet, L. Reis, J. Szabados, C. S. Werner, H. Zappe, K. Buse, and I. Breunig, Opt. Express **28**, 2939 (2020).
16. W. Yoshiki, Y. Honda, M. Kobayashi, T. Tetsumoto, and T. Tanabe, Opt. Lett. **41**, 5482 (2016).
17. S. Preble, L. Cao, A. Elshaari, A. Aboketaf, and D. Adams, Appl. Phys. Lett. **101**, 171110 (2012).
18. Y. He, H. Liang, R. Luo, M. Li, and Q. Lin, Opt. Express **26**, 16315 (2018).
19. M. Zhang, C. Wang, R. Cheng, A. Shams-Ansari, and M. Lončar, Optica **4**, 1536 (2017).
20. L. Cortes-Herrera, X. He, J. Cardenas, and G. P. Agrawal, Phys. Rev. A **103**, 063517 (2021).
21. D. Zhu, L. Shao, M. Yu, R. Cheng, B. Desiatov, C. J. Xin, Y. Hu, J. Holzgrafe, S. Ghosh, A. Shams-Ansari, E. Puma, N. Sinclair, C. Reimer, M. Zhang, and M. Loncar, Adv. Opt. Photonics **13**, 242 (2021).
22. L. He, M. Zhang, A. Shams-Ansari, R. Zhu, C. Wang, and L. Marko, Opt. Lett. **44**, 2314 (2019).
23. L. Cortes-Herrera, X. He, J. Cardenas, and G. P. Agrawal, Phys. Rev. A **106**, 023517 (2022).
24. Y. Yu, Z. Yu, L. Wang, and X. Sun, Adv. Opt. Mater. **9**, 2100060 (2021).